Vol. 88 (1995) *ACTA PHYSICA POLONICA A* No. 4

Proceedings of the XXIV International School of Semiconducting Compounds, Jaszowiec 1995

INVESTIGATION OF STRAIN IN II–VI SEMICONDUCTOR SUPERLATTICES USING ELECTRON PARAMAGNETIC RESONANCE OF Mn^{++}

J.K. FURDYNA, M. QAZZAZ, G. YANG, L. MONTES, S.H. XIN AND H. LUO†

Department of Physics, University of Notre Dame, Notre Dame, Indiana 46556, USA

We explore the possibility of using electron paramagnetic resonance (EPR) of Mn^{++} for measuring uniaxial strain in II–VI superlattices. This work is motivated by the fact that the EPR spectrum of Mn^{++} is very strongly affected by crystalline fields. Changes in a crystalline field which arise from strain are thus automatically expected to have a profound effect on the EPR spectrum. Consistent with this expectation, we have observed giant crystal field splittings of Mn^{++} EPR lines in ZnTe/MnTe, CdTe/MnTe, and ZnTe/MnSe superlattices. The EPR spectra observed in these systems are ascribed to isolated Mn^{++} ions diffused into the ZnTe or the CdTe layers from the respective MnTe or MnSe layers. In addition to providing precise information on the magnitude and the sign of strain produced by lattice mismatch between the superlattice constituents, we show that the EPR spectrum also provides a direct measure of strain fluctuations in the layered medium.

PACS numbers: 78.66.–w, 71.55.Gs

1. Introduction

Semiconductor superlattices, by their very definition, consist of alternating layers of dissimilar materials. Materials comprising these structures are, as a rule, lattice-mismatched, so that the individual layers of the superlattices are generally under considerable strain. Such mismatch-induced strain, in turn, has a profound influence on the band structure — and thus on both the optical and the electronic properties of these materials. It is therefore important to develop quantitative probes for determining strain in individual layers, in order to predict and control the band structure of the multilayer system as a whole. This is particularly important in the case of II–VI-based superlattices, where all combinations of binary

†Present address: Department of Physics, State University of New York at Buffalo, Buffalo, NY 14260, USA.

II–VI compounds, with the exception of HgTe/CdTe and ZnTe/CdSe, are highly lattice-mismatched.

In this paper we explore the potential of electron paramagnetic resonance (EPR) as a tool for determining a strain parameter in semiconductor superlattices. EPR of paramagnetic ions in a crystal lattice is strongly affected by the crystal field, which results in the well-known fine structure observed in EPR spectra at very dilute concentrations of such ions [1]. Since the presence of strain (which implies a re-arrangement of atomic positions) will clearly affect the crystal field, we have explored the question of whether the fine structure in EPR can be employed as a "strain-gauge" in the context of semiconductor multilayer systems. Conversely, investigation of EPR in strained-layer systems, where strains are larger by orders of magnitude than those produced by any conventional uniaxial pressure technique [2–5], provides an opportunity to observe the behavior of EPR in a limit not previously accessible.

We carried out our EPR investigation on ZnTe/MnTe, ZnTe/MnSe, and CdTe/MnTe superlattices, where we indeed observed enormous crystal field splittings of the EPR fine structure. The splittings are observed in the spectra of isolated Mn^{++} ions which diffused into the ZnTe or CdTe layers from the adjacent antiferromagnetic MnTe or MnSe layer, and are induced by the tensile (in the case of ZnTe/MnTe superlattices) or compressive (in CdTe/MnTe and ZnTe/MnSe) strains of the non-magnetic layers due to the lattice mismatch between neighboring materials. In addition to providing a sensitive measure of the *magnitude* and *sign* of the strain, we show that such EPR spectra also give direct quantitative information on the *strain distribution* (fluctuations) within the respective layers. This provides a direct measure of the microscopic uniformity of the multilayer structure.

2. Specimen description and experimental details

The superlattices used in this investigation were prepared by molecular beam epitaxy (MBE) using a 32 R&D Riber MBE system and elemental sources. All superlattices were grown on the (001) faces of commercial semi-insulating GaAs substrates, using a growth temperature of 310°C. Before growing ZnTe/MnTe and ZnTe/MnSe superlattices, a ZnTe buffer (typically 2 μm thick) was deposited on the substrate. Before growing CdTe/MnTe superlattices, we deposited a ZnTe buffer (typically 1 μm) followed by a CdTe buffer (about 1.5 μm). The thicknesses of all superlattices were in excess of 1 μm, so that they can be assumed to be fully relaxed, while the constituent layers (typically 120 Å or less) can be taken to be pseudomorphic. The individual layer thicknesses were determined quite precisely using reflection high energy electron diffraction (RHEED) oscillations. The EPR measurements were carried out using an X-band (9.46 GHz) Bruker ECS-106 spectrometer, with sample-cooling capability down to 4.2 K, and a goniometer for precise sample orientation with respect to the applied magnetic field.

3. Experimental results

To provide comparison for the results observed on the strained systems, we first briefly discuss the well-known EPR spectrum of an isolated Mn^{++} atom

in an unstrained II–VI host. The spectrum consists of six hyperfine-split lines separated from each other by about 60 gauss. The hyperfine splitting arises from the interaction of the magnetic moment of the Mn^{++} ion with the Mn nucleus. This is an intra-atomic process, and is thus insensitive to the host lattice surrounding the Mn^{++} ion. Each hyperfine line is in turn split into five fine structure lines by the crystal field, the fine-structure splitting depending sensitively on the crystal host, and on the angle between the applied magnetic field $\boldsymbol{H}$ and the crystal axes [6]. In ZnTe and CdTe the crystal field splittings of Mn^{++} are comparable in size to the hyperfine structure splittings, leading to relatively complex spectra. The complete spectrum, consisting of thirty lines — six hyperfine groups consisting of five fine structure lines each — typically spans about 300 gauss. We illustrate this in Fig. 1a by an EPR spectrum of Mn^{++} observed on a bulk ZnTe:Mn specimen for $\boldsymbol{H} \parallel [001]$, the orientation for which the fine structure splitting is the largest. We should note parenthetically that all "raw" spectra displayed in this paper will be in the form of absorption *derivatives*, which is the customary mode of EPR detection.

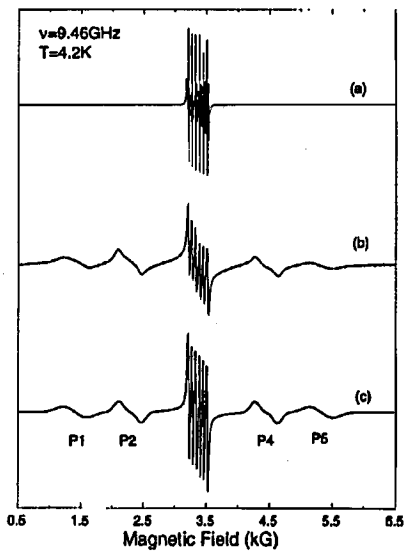

Fig. 1. EPR spectra of a very dilute Mn^{++} concentration in ZnTe for $\boldsymbol{H} \parallel [001]$: (a) observed in unstrained bulk ZnTe:Mn; (b) observed in ZnTe/MnTe superlattice SL3 (see Table); (c) calculated using $D_0 = -503$ gauss in Eq. (1) and $\Delta D = 0.07 D_0$ in Eq. (3).

We now show, in Fig. 1b, the EPR spectrum observed in a representative ZnTe/MnTe superlattice SL3 (see Table) for the external field $\boldsymbol{H}$ parallel to the growth (i.e., [001] or z) direction. Clearly this spectrum exhibits characteristically different features than that in Fig. 1a, consisting of five groups spread over a range of over 4000 gauss. These five groups actually correspond to the five fine

structure lines, each possessing six hyperfine lines. It can also be seen that the six hyperfine lines associated with the central group are well resolved, while in the other four groups they are significantly broadened. Such features are the result of an extraordinarily large fine structure splitting induced by the strain in the superlattice layers, as well as the inhomogeneous broadening of EPR lines caused by the fluctuation of this strain.

TABLE

ZnTe/MnTe and CdTe/MnTe superlattice parameters.

Sample	Sample i.d.	Layer thicknesses (in ml)			No. of periods	Strain parameter D_0	
		ZnTe	CdTe	MnTe		EPR	Neutrons*
SL1	900522A	18	–	20	100	−375	−338
SL2	940425A	16	–	20	206	−380	–
SL3	940427A	16	–	30	201	−503	−578
SL4	940627A	–	20	15	100	220	–
SL5	940628A	–	15	20	100	277	–
SL6	940727A	–	15	45	150	328	–

*As determined from neutron scattering measurements.

To facilitate discussion, we will label the five fine structure groups P_1, P_2, P_3, P_4, and P_5, ranging from the low-field (left) side to the high-field (right) side of the spectrum. As will be seen below, the relative positions of the center of each group provide a quantitative measure of the strain. The behavior observed in two other ZnTe/MnTe superlattices (SL1 and SL2) with larger ZnTe:MnTe layer-thickness ratios (see Table) is qualitatively the same as that seen in Fig. 1b, with the positions of groups P_1–P_5 being closer together due to the smaller strain in the ZnTe layers of those specimens.

4. Discussion

4.1. Spin Hamiltonian for Mn^{++} in a strained II–VI lattice

As is customary, we begin the discussion with the spin Hamiltonian for describing the spin multiplet of the ground state for an isolated Mn^{++} ion in a strained zinc-blende host crystal, given by [1]

$$\mathcal{H} = g\beta \boldsymbol{H}\cdot\boldsymbol{S} + A\boldsymbol{I}\cdot\boldsymbol{S} + \frac{a}{6}\left[S_x^4 + S_y^4 + S_z^4 - \frac{1}{5}S(S+1)(3S^2+3S-1)\right] + D_0\left[S_z^2 - \frac{1}{3}S(S+1)\right]. \quad (1)$$

The first term in the Hamiltonian is the standard Zeeman term. The second is the hyperfine structure (hfs) term, which results from the magnetic dipolar interaction of the electron spin and the nuclear spin of the Mn^{++} ion. Its only effect is to

split the spectrum into six evenly-spaced lines. Since the effect of strain on hfs is insignificant compared to strain effects on the fine structure, we will not consider it in a further analysis (except to recognize that each fine-structure line is in actuality a sextet). The third term describes the zero-magnetic-field splitting without strain (i.e., a is the zero-field fine structure splitting parameter for a relaxed zinc-blende semiconductor). The last term arises from the strain-induced axial component of the crystal field, D_0 being a strain-induced axial-symmetry parameter. For a specific strained layer of a superlattice grown along the [001] direction, D_0 is given by the following relation [7]:

$$D_0 = -\frac{3}{2}G_{11}\left(1+\frac{2C_{12}}{C_{11}}\right)\frac{a_{xy}-a_0}{a_0}, \tag{2}$$

where G_{11} is the spin-lattice coefficient describing the energy shift of spin levels per unit strain, C_{11} and C_{12} are the elastic constants, a_{xy} is the common in-plane lattice constant of the superlattice, and a_0 is the unstrained lattice constant of the material corresponding to the strained layer under consideration. By solving the secular equation associated with Eq. (1), one can find the spin levels, and thus the resonance field positions.

4.2. EPR spectrum of Mn^{++} in the $\boldsymbol{H} \parallel$ [001] orientation

It is convenient to begin by discussing the EPR spectra for the case $\boldsymbol{H} \parallel [001]$, where the fine structure splitting is the largest. For growth along the [001] direction, the strain-induced crystal symmetry is tetragonal, with the [001] direction (the z direction) being the symmetry axis. It should be noted that when the magnetic field $\boldsymbol{H}$ is parallel to the growth direction, both the Zeeman and the strain terms in the Hamiltonian are already diagonal, all off-diagonal terms being governed by a. Since in our case $a \ll D_0$, H, we can then ignore the off-diagonal elements to a very good approximation. This yields the five resonance fields for the five fine structure lines as follows:

$$\begin{aligned}
H\left(-\frac{5}{2}\rightarrow-\frac{3}{2}\right) &= H_0 + 4D_0 + 2a,\\
H\left(-\frac{3}{2}\rightarrow-\frac{1}{2}\right) &= H_0 + 2D_0 - \frac{5}{2}a,\\
H\left(-\frac{1}{2}\rightarrow\frac{1}{2}\right) &= H_0,\\
H\left(\frac{1}{2}\rightarrow\frac{3}{2}\right) &= H_0 - 2D_0 + \frac{5}{2}a,\\
H\left(\frac{3}{2}\rightarrow\frac{5}{2}\right) &= H_0 - 4D_0 - 2a,
\end{aligned} \tag{3}$$

where $H_0 = h\nu/g\beta$, ν is the microwave frequency, β is the Bohr magneton, and the numbers in parentheses denote magnetic quantum number m_s for the initial and the final state of each EPR transition (see Fig. 2). The spectrum thus provides a direct determination of the strain-induced axial symmetry parameter D_0. When hyperfine structure is included, the five resonance fields in Eq. (3) are become five sextets, P_1–P_5, seen in Fig. 1b. Taking H_0 as the center of the observed P_3 sextet,

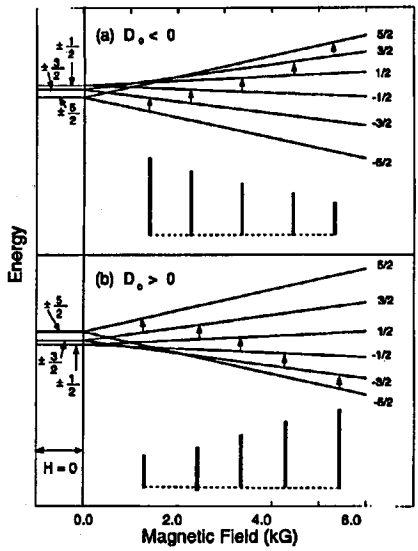

Fig. 2. Schematic illustration of the effect of strain on the fine structure splitting of the ground state of Mn^{++}, calculated (a) for $D_0 = -503$ gauss, and (b) for $D_0 = +503$ gauss. The sequence of bars below each energy diagram represents resonance positions for microwave frequency of 9.46 GHz and (qualitatively) the intensity progression of respective fine-structure lines. For clarity, the hyperfine structure is neglected.

and $a = 32$ gauss for ZnTe [5], the best fit for the resonance positions shown in Fig. 1b yields $D_0 = -(503 \pm 5)$ gauss.

The parameter D_0 can be independently evaluated from Eq. (2), and compared with the EPR result. The superlattice in-plane lattice constant a_{xy} for the same ZnTe/MnTe sample (SL3) as that used in Fig. 1b has been determined by neutron scattering [8] to be 6.230 ± 0.005 Å; the lattice constant of the unstrained ZnTe (a_0) is 6.102 Å; the spin-lattice coefficient G_{11} for Mn^{++} in ZnTe obtained from uniaxial stress experiments is 8.56 ± 0.32 kG [5]; and the elastic constants for ZnTe are $C_{11} = 7.13$ and $C_{12} = 4.88$ [9]. From these parameters, the calculated value of D_0 is -576 ± 31 gauss, in rather satisfactory agreement with the EPR result. Such a large value of D_0 indicates that the strain-induced axial symmetry of the crystal field has indeed completely dominated the fine structure splitting. For example, we see from Eq. (3) that the maximum separation between adjacent fine structure lines is about $2D_0 (\approx 1000$ gauss), more than an order of magnitude larger than the zero-strain fine structure splitting.

Taking $D_0 = -503$ gauss, $a = 32$ gauss, we show in Fig. 2a the calculated field dependence of the spin levels for the magnetic field parallel to the growth direction. (For the sake of clarity, hyperfine splitting is not shown in the figure.) At zero magnetic field, the six-fold degenerate ground state of Mn^{++} is split into three doublets by strain, with separations of $4D_0 + 2a$ (between $\pm\frac{5}{2}$ and $\pm\frac{3}{2}$ levels) and $2D_0 - \frac{5}{2}a$ (between $\pm\frac{3}{2}$ and $\pm\frac{1}{2}$). In the presence of a magnetic field, all

degeneracies are removed for this orientation. Figure 2a also shows (by arrows) the calculated resonance fields at which the five fine structure absorption lines occur for $g = 2.0106$, $a = 32$ gauss [5], $D_0 = -503$ gauss, and a microwave frequency of 9.46 GIIz. Figure 2b shows that the resonance fields would be the same for $D_0 = +503$ gauss (compressive) as for $D = -503$ gauss (tensile strain).

4.3. Strain fluctuations

As discussed above, the EPR line positions (Eq. (3)) provide a measure of the magnitude of the strain, as expressed through D_0. The *resolution* of the hfs lines within each group P_i, on the other hand, provides a direct quantitative measure of *strain fluctuations*. That is, in the presence of some strain non-uniformity (either along the growth direction, or laterally across the layers), there will automatically follow a distribution of resonance fields for each strain-shifted fine-structure line ("inhomogeneous" broadening) [10, 11]. This can be immediately seen from Eq. (3) where, for the same strain fluctuation, the inhomogeneous broadening for branches P_1 and P_5 is twice as large as for P_2 and P_4.

To simulate such broadening associated with strain fluctuation, we assume that the strain-induced fine structure splitting parameter D has a Gaussian distribution around its average value D_0

$$P(D) = A \exp\left[-0.693 \frac{(D - D_0)^2}{(\Delta D)^2}\right], \tag{4}$$

where $P(D)$ is the probability for a specific value of D, and ΔD is the half width of the Gaussian strain distribution, which can be fitted to the experimental EPR linewidths. When $\boldsymbol{H}$ is parallel to the growth direction, the inhomogeneous broadening of the linewidths in each fine-structure group P_i can thus be obtained by using the Gaussian distribution of D given by Eq. (4) directly in Eq. (3). It is easy to see that the linewidths of the individual EPR lines due to strain fluctuation are $4\Delta D$ for P_1 and P_5, $2\Delta D$ for P_2 and P_4, and 0 for P_3 branch.

The spectrum shown in Fig. 1c has been calculated using the already established value of $D_0 = -503$ gauss, literature values of $a = 32$ gauss and $A = 60$ gauss for fine- and hyperfine-splitting constants for Mn^{++} in ZnTe [5], a strain distribution parameter $\Delta D = 0.07 D_0$ (see Eq. (4)), and an intrinsic linewidth of 23 gauss taken from the measured width of the individual lines in the central sextet P_3. As can be seen, excellent agreement is found between the calculated and the experimental spectrum. It is important to note that only two adjustable parameters (apart from the measured intrinsic linewidth) were used in calculating this spectrum: D_0 and ΔD, one of which determines the positions of the P_i groups, the other their shape.

4.4. Angular variation of EPR

As was already remarked, the EPR spectrum of Mn^{++} is a highly sensitive function of the angle between $\boldsymbol{H}$ and the crystallographic axes. The analysis of this angular dependence is in the present case considerably more complicated than was the preceding discussion of the symmetric situation $\boldsymbol{H} \parallel [001]$, because of the need to include off-diagonal terms in the diagonalization of Eq. (1) for $\theta \neq 0$ (where

θ is the angle between $\boldsymbol{H}$ and the [001] axis). Here we will only discuss the new features associated with strain in qualitative terms, leaving details for a more extensive presentation.

Briefly, we investigated the angular variation for $\boldsymbol{H}$ in the (110) plane (which contains the growth direction). We define the orientation $\boldsymbol{H} \parallel$ [001] already discussed as $\theta = 0$. As the magnetic field is tilted away from [001], it is observed that positions of P_1 and P_5, and P_2 and P_4, which are symmetric around P_3 in the absence of strain [6], lose this well-known symmetry when strain is present. For example, in the unstrained cubic case all fine structure lines collapse for one value of $\theta = 31°43'$, but this is no longer so in the present case.

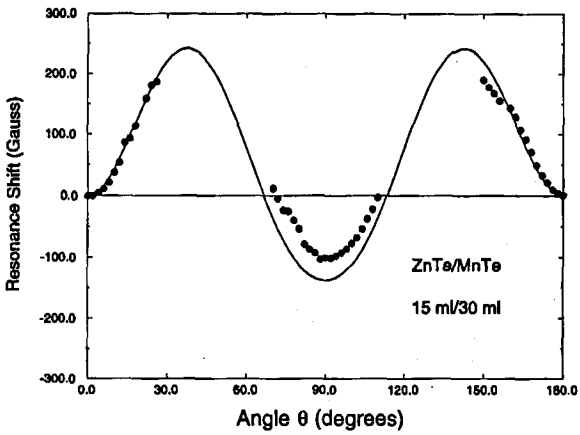

Fig. 3. Angular dependence of the center of the P_3 branch, for $\boldsymbol{H}$ in the (110) plane in ZnTe/MnTe superlattice. $\theta = 0$ corresponds to $\boldsymbol{H}$ parallel to the growth direction, [001]. Solid curve is calculated using $D_0 = -503$ gauss; points are experimental for sample 3. Overlap of other fine structure branches with P_3 prevents reliable determination of the P_3 position in the regions between 30° and 70°, and 110° and 150°.

Furthermore, while in the unstrained case the magnetic field positions of the group-P_3 lines (corresponding to the $-1/2 \rightarrow 1/2$ transitions in Fig. 2) remain independent of θ, in the case of strained layers these lines also shift quite significantly with an angle. This is perhaps the most striking (and useful) feature of the angular dependence of the strained systems. We illustrate this in Fig. 3, where the position of the central fine structure group (P_3) observed for sample SL3 is plotted as a function of the angle between $\boldsymbol{H}$ and [001]. The solid line is the calculated result using the already established value of $D_0(-503$ gauss) in the spin Hamiltonian, Eq. (1). As can be seen, the calculated angular dependence of the resonance field agrees very well with our experimental data. (The gaps in the data for $30° \leq \theta \leq 70°$ and $110° \leq \theta \leq 150°$ in the figure arise from the fact that in these regions the various branches P_i overlap, making the identification of the P_3 positions unreliable.) The above differences in angular dependence between the unstrained and the strained cases arise from the fact that in the latter situation

we have in fact an axially-symmetric rather than a cubic crystalline field. Thus the angular dependence (e.g., Fig. 3) provides an independent measure of strain. This may be especially important in cases where strain fluctuations are large, such that the central sextet P_3 is frequently the only resonance feature which survives.

4.5. The sign of D_0

So far we have only concentrated on the magnitude of D_0. Measurement of the relative intensity of the branches $P_1, \ldots, P_5$ at low temperatures also provides a way for the determination *of the sign* of D_0, as can be seen while considering Fig. 2. Since the relative populations of the various levels differ at low temperatures [12], then the intensities of the absorption lines will be strongest for those lines whose initial states lie lower in energy. For example, for $D_0 < 0$, the $-5/2$ level will be more populated at low temperatures than the $5/2$ level, etc. As illustrated in Fig. 2a by the vertical bars, we then expect that the low-field fine structure groups (the P_1 and P_2 sextets) will be stronger in intensity than the fine structure groups occurring at high fields (P_4 and P_5). Close inspection of Fig. 1 reveals that this is exactly the case for our ZnTe/MnTe sample.

We have also carried out EPR measurements on three CdTe/MnTe superlattices with various relative thicknesses of the CdTe and MnTe layers, and on one ZnTe/MnSe superlattice. The CdTe/MnTe spectra, observed for $\boldsymbol{H} \parallel [001]$, are

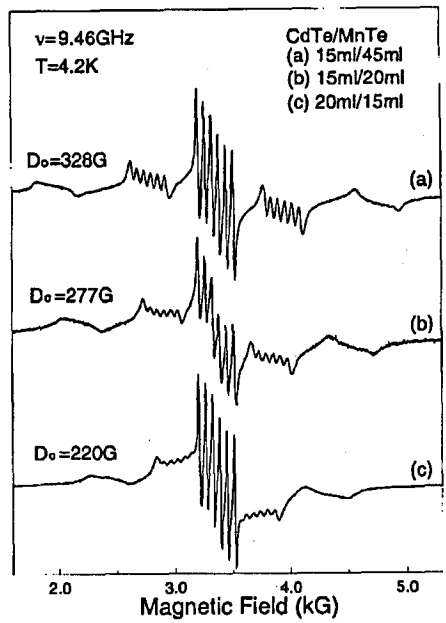

Fig. 4. EPR spectra for three CdTe/MnTe superlattices (samples SL4, SL5, and SL6 in Table), in sequence from the most highly strained (top) to the least strained CdTe layers (bottom), observed for $\boldsymbol{H} \parallel [001]$.

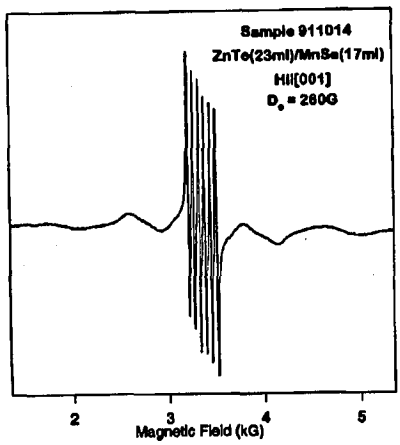

Fig. 5. EPR spectrum for a ZnTe/MnSe superlattice observed for $\boldsymbol{H} \parallel [001]$. The layer thicknesses are shown in the figure in monolayers, along with the value of D_0 obtained from the EPR line positions.

shown in Fig. 4 in sequence of decreasing strain in the CdTe layers, as inferred from the relative CdTe-to-MnTe layer thicknesses (given in the figure in monolayers; see also Table). As expected, the fine structure splitting decreases as the strain in the CdTe layers decreases, and the resulting values of D_0 obtained from the splittings are shown in the figure for each sample. The EPR spectra ($\boldsymbol{H} \parallel [001]$) for the ZnTe/MnSe superlattice are shown in Fig. 5. A close inspection of Figs. 4 and 5 also reveals that, in contrast to Fig. 1, now the high-field branches P_4 and P_5 are stronger at low temperatures than the low-field branches P_1 and P_2. This indicates that D_0 is *positive* since, as can be seen in Fig. 2b, for $D_0 > 0$ the stronger transitions $-5/2 \rightarrow -3/2$ would occur at the highest field, $3/2 \rightarrow 5/2$ at the lowest, etc. This indicates that the layers containing the dilute Mn^{++} populations responsible for the observed resonance (i.e., CdTe or ZnTe) are now under *compressive* strain. Note also the degree of resolution in spectrum (a) of Fig. 4 (corresponding to sample SL6 in Table), in which hfs is nearly resolved even for P_5. This indicates a remarkable uniformity of strain throughout the sample. In comparison, the resolution in the ZnTe/MnSe system is the poorest of the samples described in this paper.

4.6. Temperature dependence of the EPR linewidth

Before concluding we wish to note that the EPR *linewidth* — and especially its temperature variation — carry valuable information concerning magnetic interactions between the Mn^{++} magnetic spins. This has been clearly demonstrated for concentrated unstrained systems (e.g., $Cd_{1-x}Mn_xTe$ and $Zn_{1-x}Mn_xTe$ for $x > 0.10$), where the linewidth exceeds both fine structure (fs) and hyperfine structure (hfs) splittings [13, 14]. For very dilute systems the EPR spectrum will be automatically complicated by the presence of the fs and hfs effects, making the lineshape extremely difficult to analyze and interpret.

It is therefore worth noting that the strained-layer structures, such as those discussed above, offer a valuable advantage in this context. By removing the fine structure satellites P_1, P_2, P_4, and P_5 far away from the $-1/2 \rightarrow 1/2$ transition, the strain leaves a much "cleaner" spectrum, with only hfs present. This makes it possible to determine quantitatively the changes in the linewidth on the scale of a few gauss. We thus have the important opportunity to investigate the effect of distant magnetic neighbors on the linewidth, at concentrations where Mn^{++}–Mn^{++} interactions just begin to take effect.

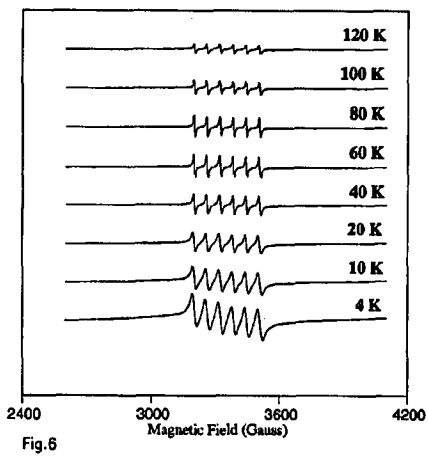

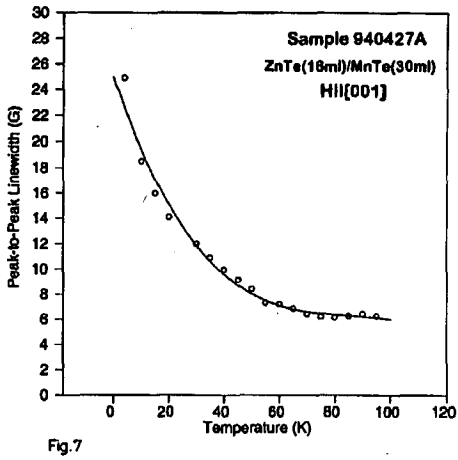

Fig. 6. Progression of the P_3 branch of the EPR spectrum for SL3, $\boldsymbol{H} \parallel [001]$, observed for a series of temperatures.

Fig. 7. Temperature dependence of the linewidth (peak-to-peak) of individual lines comprising the P_3 branch for SL3, obtained by fitting the data shown in Fig. 6.

We illustrate this by the temperature dependence of the central EPR manifold (the P_3 branch) of SL3, shown in Fig. 6. Note that the widths of the individual lines become clearly narrower as the temperature increases (as indeed they do at high values of x, see Refs. [13, 14]). The temperature dependence of the linewidth obtained from fitting these data is shown in Fig. 7. A detailed analysis of the linewidth is beyond the intended scope of this paper. Our intention at this point is merely to point out yet another interesting aspect of EPR in systems under extremely high uniaxial strain.

5. Concluding remarks

Finally, we wish to comment on the assumption made at the outset that the resonance which we observe is due to Mn^{++} ions present (in very dilute amount) in the nonmagnetic layers (CdTe or ZnTe) of the superlattices, having entered these layers by diffusion from MnTe or MnSe in the various structures investigated. This assumption, made a priori, is reasonable, since EPR in systems with high concentrations of Mn (including the antiferromagnetic MnTe or MnSe) is broadened to

oblivion [13]. We remark now that this assumption is fully verified a posteriori both by the progression of the fine structure splitting, which increases with increasing strain in the non-magnetic layers (see, e.g., Fig. 4 and Table), and by the respective signs of D_0 observed for ZnTe and CdTe under tensile or compressive strain. We should remark that these spins have found themselves in their respective non-magnetic hosts "by accident", providing us with a convenient opportunity to investigate the effect of strain on EPR. These results clearly suggest that dilute amounts of Mn can be introduced into selected layers of fully non-magnetic II–VI superlattices (e.g., ZnTe/CdTe), so as to use EPR as a "strain gauge" for the layers containing Mn. We are now systematically pursuing this promising direction.

Acknowledgments

We thank U. Bindley and S.W. Short for help in the MBE growth of the specimens used in this research. This work was supported by the NSF/MRG grant DMR92-21390.

References

[1] W. Low, *Paramagnetic Resonance in Solids*, in series *Solid State Physics*, Eds. F. Seitz, D. Turnbull, Suppl. 2, Academic Press, New York 1967, Chap. 2.

[2] E. Feher, *Phys. Rev. A* **136**, 145 (1964).

[3] D. Boulanger, R. Parrot, *Phys. Status Solidi B* **140**, K79 (1987).

[4] R. Parrot, C. Blanchard, D. Boulanger, *Phys. Lett. A* **34**, 109 (1971).

[5] M.T. Causa, M. Tovar, S.B. Oseroff, R. Calvo, W. Giriat, *Phys. Lett. A* **77**, 473 (1980).

[6] L.M. Matarrese, C. Kikuchi, *J. Phys. Chem. Solids* **1**, 117 (1956).

[7] G. Yang, *Electron Paramagnetic Resonance in II–VI Semiconductor Heterostructures*, Ph.D. Thesis, University of Notre Dame, 1993 (unpublished).

[8] T.M. Giebultowicz, private communication.

[9] D.A. Berlincourt, H. Jaffe, L.R. Shiozawa, *Phys. Rev.* **129**, 1009 (1963).

[10] A.M. Stoneham, *Rev. Mod. Phys.* **41**, 82 (1969).

[11] R. Parrot, G. Tronche, *Phys. Status Solidi* **41**, 217 (1970).

[12] S.A. Marshall, in: *Optical Properties of Solids*, Eds. S. Nudelman, S.S. Mitra, Plenum Press, New York 1969, p. 548.

[13] N. Samarth, J.K. Furdyna, *Phys. Rev. B* **37**, 9227 (1988).

[14] Z. Soskic, B. Babic Stojic, M. Stojic, *J. Phys.; Condens. Matter* **6**, 1261 (1994).